ELSEVIER

Weathering profile of non-welded ignimbrite and the water infiltration behavior within it in relation to the generation of shallow landslides

Masahiro Chigira[a,*], Osamu Yokoyama[b]

[a]*Disaster Prevention Research Institute, Kyoto University, Gokasho, Uji 611-0011, Japan*
[b]*Japan Conservation Engineers, 4-4-1 Sanbancho, Matsuyama 790-0003, Japan*

Abstract

The mechanism underlying rain-induced shallow landslides of non-welded ignimbrite is found to be a special type of weathering profile and the behavior of water infiltrating through that profile, according to our study of Ito ignimbrite in southern Kyushu, Japan. Rhyolitic volcanic glass, the primary component of ignimbrite, is first hydrated and dissolved, forming halloysite. Halloysite near ground surface is then transported through the ignimbrite by infiltrating water and becomes clogged in interstices to form clay bands. Suction monitoring across a weathering profile indicated that downward infiltration of water is disrupted once by a zone of less-permeable clay bands and again at the weathering front. This disruption at the front is caused by a capillary barrier effect caused by the structure where finer, weathered material overlies coarser, fresh material. This results in a well-defined weathering front, particularly beneath a slope where water flux is parallel to the front, whereas the front is transitional beneath a ridge top where the front is nearly horizontal and the water flux is normal to the front. Infiltrating water from rain increases the weight of weathered material and decreases the suction within the material, which is the final trigger of a shallow landslide of non-welded ignimbrite; long-term weathering, which proceeds on the order of years, provides slide material.
© 2005 Elsevier B.V. All rights reserved.

Keywords: Ignimbrite; Weathering; Landslide; Soil moisture

1. Introduction

The weathering of rocks has been studied in various scientific fields, such as geology, engineering geology, mineralogy, soil science, and geomorphology. But the relationship between the weathering and the occurrence of landslides has not been well understood. This is because the previous studies focused on partial elementary processes rather than on sequential and interconnected weathering processes. Consequently, weathering profiles are not well characterized or understood, while soil profiles, which

* Corresponding author. Fax: +81 774 38 4100.
E-mail address: chigira@slope.dpri.kyoto-u.ac.jp (M. Chigira).

form the upper part of weathering profiles, have been studied in many countries. Although recent studies advanced the understanding of water–rock interaction, which is the most important process for the formation of a weathering profile, they focused mostly on chemical reactions rather than the characterization or interpretation of weathering profiles. Some researchers have made geochemical models of reaction and advection (Phillips, 1991; Lichtner et al., 1996; Lasaga, 1998), but those models are still conceptual and have not fully explained weathering profiles in nature. The characterization of weathering profiles used to be performed by geotechnical or engineering geological researchers (Moye, 1955; Ruxton and Berry, 1957; Geological Society, 1995) because they have to know the profiles to evaluate the geometrical distribution of mechanical properties of rocks as foundations. Weathering profiles have been studied for the following: granite (Moye, 1955; Ruxton and Berry, 1957; Chigira, 2001), marine sedimentary rocks (Chigira, 1990; Chigira and Sone, 1991; Chigira and Oyama, 1999; Hachinohe et al., 1999; Oyama and Chigira, 1999), vapor-phase crystallized ignimbrite (Chigira et al., 2002), and non-welded ignimbrite (Shimokawa et al., 1989; Yokota and Iwamatsu, 1999;

Kawano and Tomita, 1999). These studies showed that each rock type has specific weathering profiles, which can be explained by geological processes. This geological characterization and interpretation of weathering profiles must be performed much further to establish a methodology of extending very limited data obtained by drilling, geophysical prospecting, or monitoring to a wider area on the basis of generality of geological processes.

Pyroclastic flow deposits (i.e., ignimbrite), one of the most common pyroclastics in tectonically active regions (Cas and Wright, 1996), have been prone to landslides during heavy rainfalls. For example, Shirasu, which is a local name of typical non-welded and unconsolidated ignimbrite in Kagoshima and is described in this paper, has been involved in shallow landslides on many occasions, resulting in numerous casualties (Fig. 1, Yokota and Iwamatsu, 1999; Yokoyama, 1999); this situation is generally expected in ignimbrite areas in humid regions. Shirasu weathers so quickly that, after a landslide strips off the surface weathered layer, weathering recommences and quickly provides material for the next landslide (Shimokawa et al., 1989; Yokota and Iwamatsu, 1999). The migration of a weathering

Fig. 1. Landscape in Kagoshima Prefecture, showing the shallow landslides of 1993 (photo by Kokusai Koku Photo).

front and the deterioration within the weathering zone proceed on the order of years, providing 60-cm-thick weathering zone in about 130 years (Shimokawa et al., 1989). Recurrence interval of landslides is thus inferred to be on the order of tens of years to a few hundred years. At present, the weathering mechanism of non-welded ignimbrite has not been elucidated sufficiently, but it is supposed to be dominated by chemical interactions between Shirasu and groundwater. Such a process is indicated by the increase in water content toward the ground surface and the formation of halloysite (Shimokawa et al., 1989; Kawano and Tomita, 1999; Yokota and Iwamatsu, 1999). Geochemical studies indicate that volcanic glass is easily weathered by hydration, ion exchange, dissolution, and clay mineralization (Petit et al., 1990; Yanagisawa et al., 1997). Yokota et al. (1997) monitored the water infiltration behavior within Shirasu by using automated electrical prospecting. They found that water infiltrates downward gradually and that the cycle of wetting and drying repeats intensely in the shallower part. However,

water infiltration behavior has not been monitored directly before by using tensiometers or measuring equipment of water contents.

This paper characterizes the weathering profile of Shirasu as a typical non-welded ignimbrite, then discusses the water infiltration behavior based on the monitoring of suction within a weathering profile, and finally refers to the initiation of a landslide.

The study area is located in the east of Kagoshima Prefecture in southern Kyushu Island (Fig. 2). Kagoshima Prefecture is widely covered by Shirasu, the non-welded part of Ito ignimbrite with an age of 24,500 years before the present (Yokoyama, 1999). In and around the study area, Shirasu has its depositional flat top surface, whose elevation ranges from 100 to 200 m and which is dissected by streams. We selected three sites in the study area to observe and analyze weathering profiles and to monitor the water infiltration behavior within each weathering profile of Shirasu. These three sites are within an area of about 1 km^2 (Fig. 2), and include Niitome (site N), Tsukino (site T), and Iwamoto (site I).
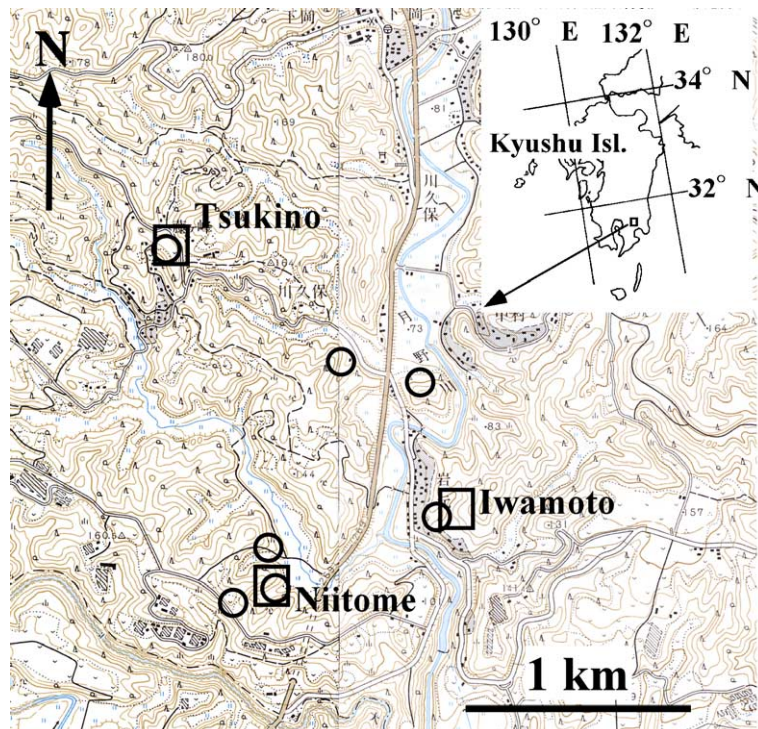
Fig. 2. Index map of the study area. Circles indicate the outcrops where clay bands were observed. The base maps are of Osumi–Matsuyama and Nogata with a scale of 1:25,000 and are made by the Geographical Survey Institute, Japan.

2. Methods

Weathering profiles were observed at artificial cross cuttings made for the construction of roads or houses at sites N and T, and suction monitoring was made at a natural slope of site I. At sites N and T, physical properties such as soil hardness, density, porosity, and water content were measured, and mineralogical identification was made. In addition, we analyzed particle size distribution and observed the surface textures of glass fragments from among the samples from site N.

Soil hardness was measured by using a portable hardness tester (Soil hardness meter, Yamanaka type, Daiki Rika Kogyo Co., Japan). Soil hardness is measured as a resistance against the penetration of a cone of a standardized specification (Yokota and Iwamatsu, 1999). The apex angle of the cone is $25°20''$ and the spring resilience is 8 kgf/40 mm. The soil hardness index is obtained as the depth of penetration when a cone is pushed by a spring. This index is related to soil strength, as mentioned later. At each measuring point on a cut slope, the loosened surface layer was scraped off before soil hardness was measured. Because this measurement disturbs the soil structure and the neighboring measurement points were close to each other (10-cm intervals), measurement was taken once at one point. Dry bulk density, solid density, and porosity were calculated by means of weight, bulk volume, and net volume; the net volume was measured for powdered samples by use of an air-pycnometer, a Micromeritics multi-volume pycnometer 1305, and the bulk volume was measured as the volume of sand replacing in situ a mass of Shirasu whose weight had been measured. Water content was measured by the following process. Samples were powdered and dried in a dessicator for 2 or more days and weighed to obtain their weight (W_1) under room conditions. They were heated to 110 °C repeatedly until their weights (W_2) did not change, then heated again to 800 °C repeatedly to get constant weights (W_3). Water content H_2O^- is $(W_1-W_2)/W_1$ and H_2O^+ is $(W_2-W_3)/W_1$. Particle size distribution was measured by the sieving and settling method.

X-ray diffraction analysis was performed for the clay fractions obtained by the settling method. The Rigaku RAD-BII was used under the conditions of Cu(Kα), 40 kV, 20 mA, and a scanning speed of 0.5°/min or 0.25°/min. Ethylene glycol treatment and heating to 300 °C were used to identify clay minerals.

Surface textures of glass grains were observed by using a scanning electron microscope, the JEOL JSM5400LV. The samples were ultrasonically rinsed with distilled water. Glass grains were picked by hand under the optical microscope and then observed with the scanning electron microscope at magnifications up to 5000.

Suction was monitored at two points 5 m apart on a slope in site I by using the DIK-3021 tensiometer produced by Daiki Rika Kogyo Co. We drilled auger holes and characterized the weathering profile, then set the tensiometers. At both points, the porous cups were 50, 100, 150, and 200 cm deep. The data were sampled at intervals of 10 min. The monitoring period was 23 August to 1 October 2001. Precipitation was also measured by using a tipping-bucket rain gauge set between the two tensiometer nests. The geology of the monitoring site is described later with reference to the relative positions of the porous cups of the tensiometers and the weathering zone.

3. Results and discussion

3.1. Weathering profile

In these study sites, Shirasu is composed mainly of rhyolitic volcanic glass of sand and silt sizes with pumice fragments up to 5 cm in diameter, plagioclase, quartz, pyroxene, and small amounts of lithic fragments. The weathering zone of Shirasu has generally been classified into three zones (IIa, IIb, and IIc) according to color, hardness judged from hand inspection, and texture (Fig. 3). Shirasu in zone I, a fresh zone, is bright gray and can be penetrated by a hammer pick, but it is also dense, which the soil hardness index will indicate. The pumice grains in zone I cannot be broken by hand. They protrude on a cut slope because they are resistant to erosion by rainwater. Shirasu in zone II is weathered and the pumice grains in it can be crushed by hand. The pumice grains within this zone are weak and do not protrude on a cut slope. Shirasu in zone IIa is not discolored and has no clay bands, which will be described later. Shirasu in zone IIb is discolored into
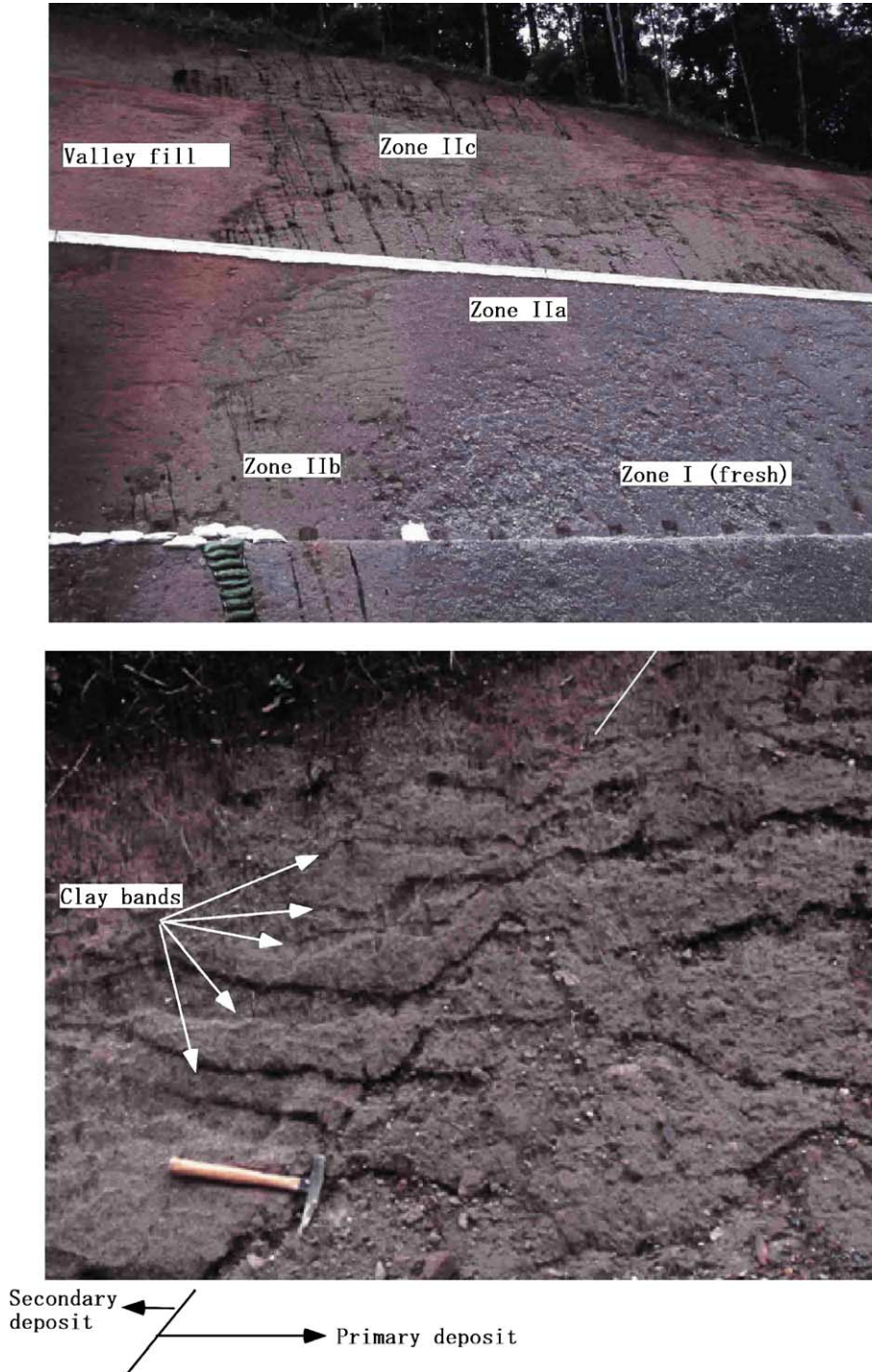
Fig. 3. Typical weathering profile of Shirasu at site N. Above: weathering zones. Below: clay bands crossing the boundary between the primary deposit of Shirasu and its secondary deposit.

pale brown (dark brownish gray when it is wet) and has a few clay bands in an interval of 1 m. Shirasu in zone IIc is also discolored into pale brown but has many more clay bands than IIb (5 to 10 bands in an interval of 1 m).

A clay band is a layer with thickness ranging from a few to 5 cm and a length of about 30 cm to 2 m, where the halloysite-rich clay fraction is concentrated within interstices among original grains (Fig. 3). When a clay band is in contact with large pumice fragments, it always mantles the upper periphery of fragments, showing that the fine fraction migrated downward and covered it as will be shown in Fig. 5. In addition, some clay bands extend across the boundary between original Shirasu, pyroclastic flow deposit, and its secondary deposits on a slope (Fig. 3). These characteristics indicate that the clay bands formed after the deposition of Shirasu, and that the bands were not a primary texture during the time of the ignimbrite deposition. These two findings indicate that clay bands were

formed by the transportation of a fine fraction by downward-infiltrating water and by the clogging of Shirasu's interstices.

The weathering of non-welded ignimbrite has been studied by only a few researchers (Shimokawa, 1984; Yokota and Iwamatsu, 1999; Kawano and Tomita, 1999). In all of those studies, the subject material was Shirasu. Although they examined the soil hardness and/or mineralogy, none recognized that the weathering zone may be divided into IIa, IIb, and IIc. However, we carefully inspected many outcrops in addition to the sites described in this paper, and we found that this classification can be generally applied to Shirasu.

Weathering profiles of Shirasu were observed at a cut slope about 150 m wide and 15 m high at site N, and at a cut slope about 70 m wide and 15 m high at site T. The weathering profiles of sites N and T have similar characteristics: zones I, IIa, IIb, and IIc appear in this order from the depth to the ground surface, although some zones are present locally (Fig. 4). At
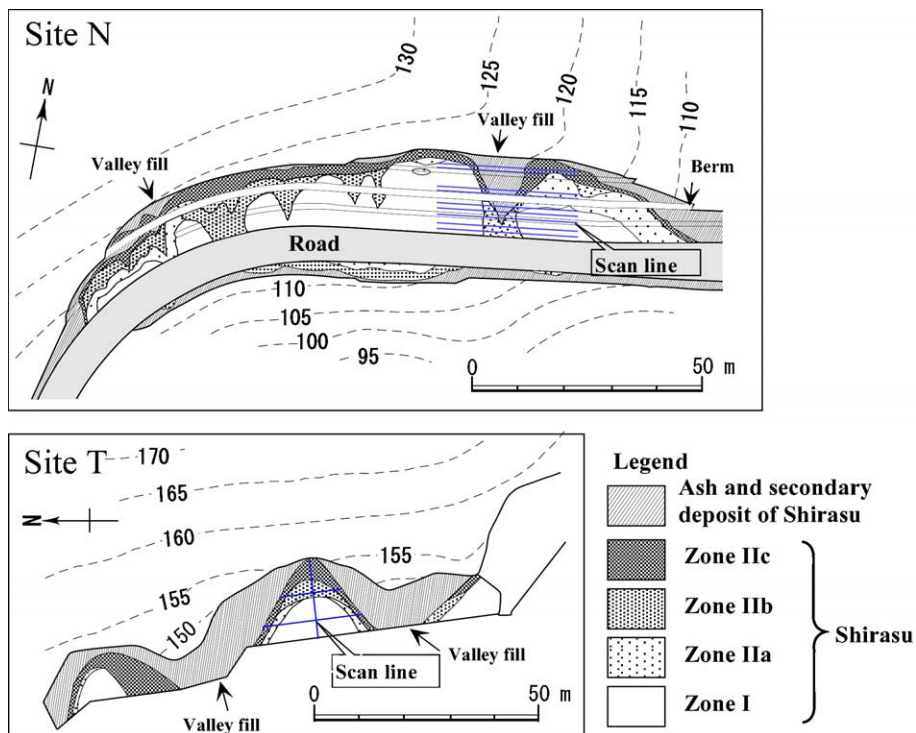
Fig. 4. Weathering profiles at sites N and T.

site N, zone IIb was observed to protrude in down-ward wedges in 6 locations. These protrusion loca-tions seem to be below old small valley bottoms (Fig. 4), which had been subsequently filled with ash. At site T, the parts below the small valleys were not observable.

3.2. Physical property changes

Scanning lines for the measurement of physical and related properties across the weathering zones were set at sites N and T (Fig. 5). Horizontal scanning lines were set on artificial cut slopes across a buried
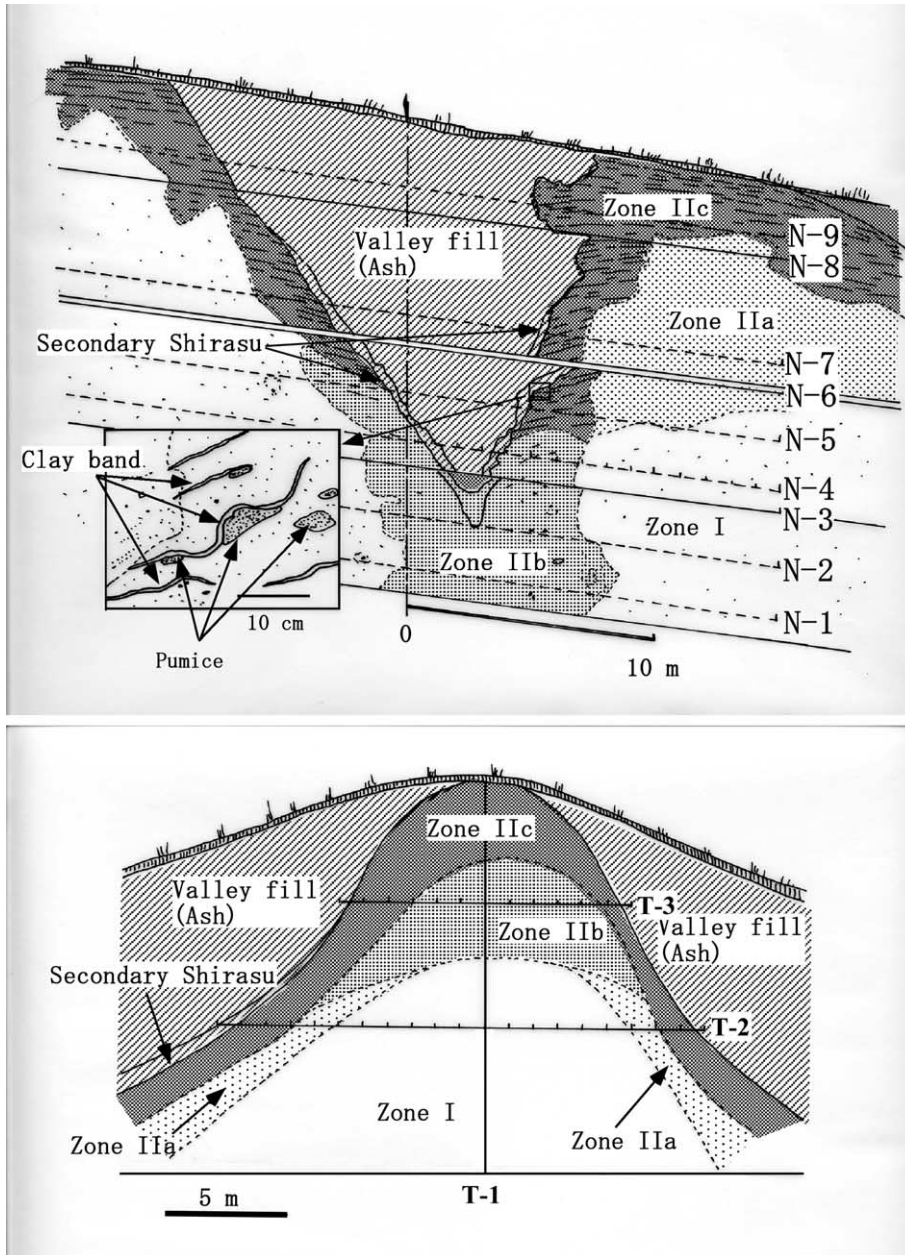
Fig. 5. Scanning lines for the measurements and analyses of soil properties at sites N and T.

valley and a ridge at sites N and T. An additional scanning line, T-1, was set within a vertical section along a ridge axis at site T, so that the physical property change could be observed beneath a ridge top. The buried slope surfaces inclined at about 60°. At site N, soil hardness was measured along six horizontal scanning lines N-1, N-2, N-4, N-5, N-7, and N-9 in Fig. 5; and physical properties, such as density and porosity, were measured along one scanning line N-3, 1 m below line N-4. At site T, soil hardness was measured along all the lines, T-1,

T-2, and T-3, and physical properties were measured along T-1 line. After the investigation at site N was completed, the local government planted grass along the cut surface. This is a common practice to protect artificially cut slopes of Shirasu from soil erosion. After this planting, investigation within a vertical section was no longer possible at site N.

Physical properties changed across the base of a weathering zone, which is a weathering front, and the changing patterns differed between a profile beneath a slope and a profile just beneath a ridge top. The
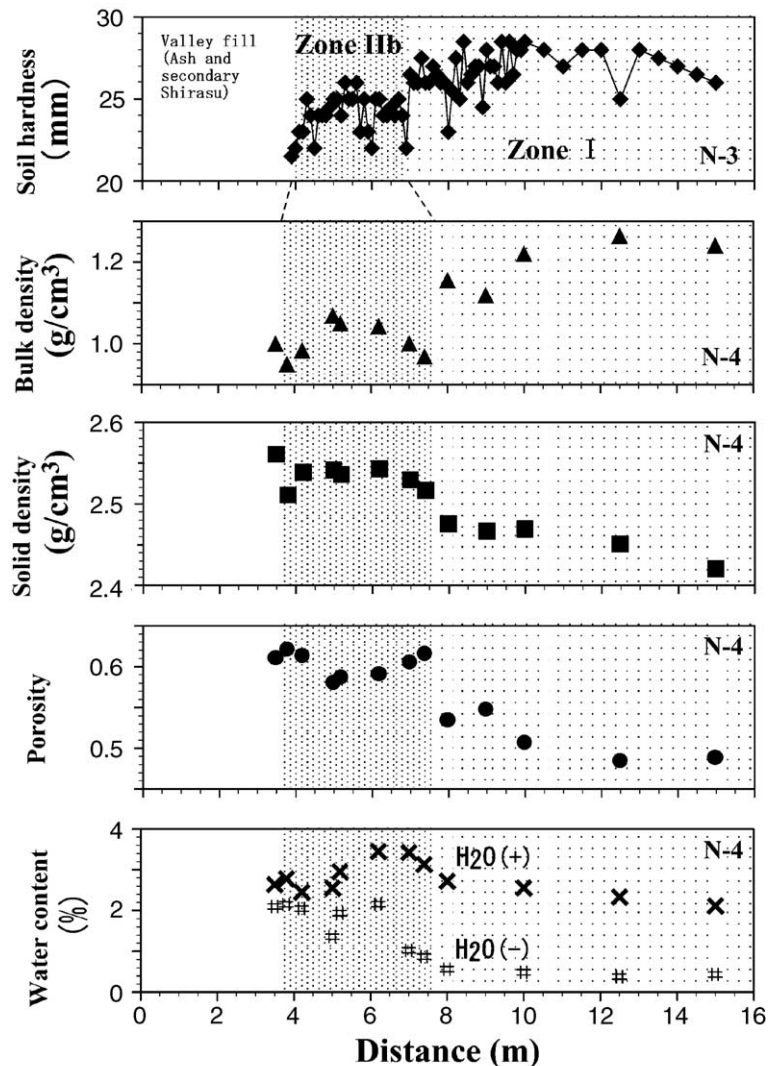
Fig. 6. The change of soil hardness indices along line N-4 and the change of other physical properties along line N-3 at site N. These two lines are parallel and 1 m apart.

patterns changed abruptly across the front beneath slopes, but gradually across the front beneath a ridge top. Fig. 6 shows the typical changes of physical properties (soil hardness, bulk density, solid density, porosity, and water content) along lines N-3 and N-4 across the weathering zones beneath the slope at site N. Soil hardness, which was measured at 10-cm intervals along the scanning lines, fluctuates a few to 5 mm between the neighboring points, but its average decreases abruptly from values of about 27 mm in zone I to about 24 mm in zone IIb along scanning line N-4 (Fig. 6). Correspondingly, along line N-3, 1 m below line N-4, the average bulk density decreases from 1.2 g/cm³ in zone I to 1.0 g/cm³ in zone IIb;

solid density increases from 2.47 g/cm³ to 2.53 g/cm³; porosity increases from 0.54 to 0.60; and $H_2O(+)$ increases from 2.6% to 3.2% then apparently falls back to 2.7%. Based on the formation of halloysite from volcanic glass by weathering, as described later, we infer that solid density increases with weathering; the specific gravity of halloysite is 2.55 (Deer et al., 1966) and that of rhyolitic volcanic glass is 2.37 (Daily et al., 1966). Such abrupt changes in the soil hardness index from zones I to IIb were observed along all the scanning lines. The boundary between zones I and IIa was crossed by only one scan line, where the line and the boundary were subparallel, so the change from zones I to IIa was not clearly
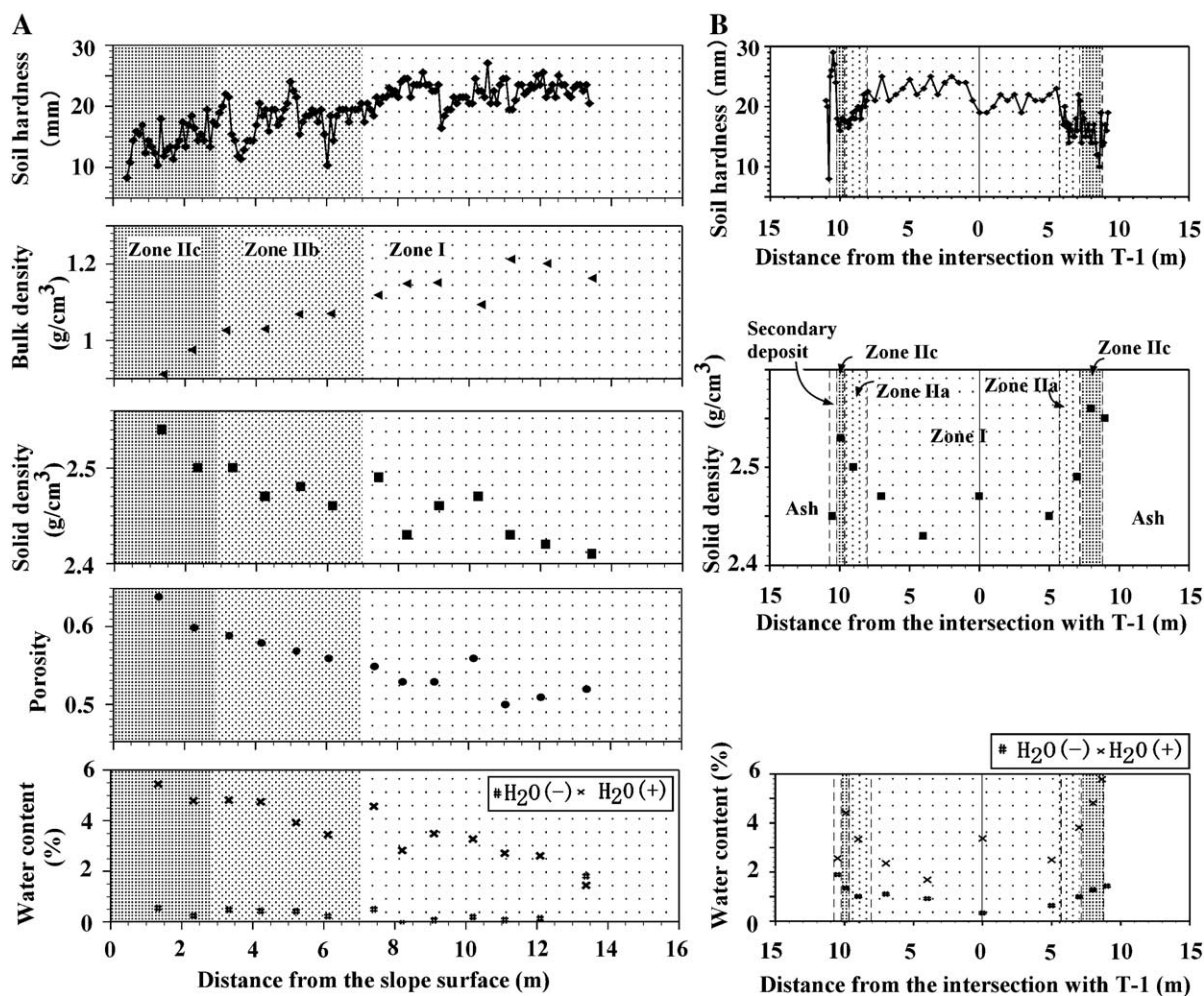
Fig. 7. The change of soil indices and physical properties along line T-1 at site T (A) and along horizontal line T-2 (B).

detected. However, the change from zone I to IIa was observed to be abrupt at site T, as described later. There are no data on the physical properties of Shirasu within zone IIa, but its soil hardness indices were 23 mm on average and about the same as those of Shirasu in zone IIb, so its physical properties are inferred to be similar to those of Shirasu in zone IIb.

The physical property changes across a weathering front beneath a ridge top were rather gradual in comparison with the changes observed across a weathering zone beneath a slope. Fig. 7A shows the changes in physical properties along T-1 line within a vertical cross-section at site T. The soil hardness index fluctuates from 5 to 10 mm between neighboring points, and its average decreases gradually from 23 mm in mid-zone I to about 19 mm in mid-zone IIb, and then to 14 mm in mid-zone IIc. Correspondingly, bulk density decreases from 1.18 g/cm^3 in mid-zone I to 1.06 g/cm^3 in mid-zone IIb, and then to 0.96 g/cm^3 in mid-zone IIc; solid density increases from 2.42 g/cm^3 to 2.48 g/cm^3 and then to 2.52 g/cm^3; and porosity increases from 0.51 to 0.57, then to 0.61. $H_2O(+)$ increases 3.0% to 4.0%, then 5.0%. In contrast to the change beneath the ridge top, the change along a horizontal scanning line across a slope was abrupt at the weathering front (T-2, Fig. 7B), as was the case at site N. Average soil hardness indices decreased abruptly from 21 mm in zone I to 18 mm in zone IIa along the T-2 horizontal

scanning line. Solid density and water content also changed abruptly along this scanning line. Soil hardness indices of Shirasu in zone IIa obtained at horizontal scanning lines were 18 mm on average, about the same as those in zone IIb, so Shirasu in zone IIa is inferred to have similar physical properties as those in zone IIb.

Physical properties, particularly soil hardness indices in zone I, differ slightly between sites N and T, as is seen in Figs. 6 and 7. This may be attributed to the variation of original physical properties from site to site at the time of Shirasu deposition.

Particle size analyses were performed for the samples from site N. Particle size distributions of Shirasu from zones I, IIa, IIb, and clay bands in zone IIc are shown in Fig. 8. Fractions coarser than 1.68 mm in diameter occupied 10 to 20 wt.%, but these proportions depend strongly on the original heterogeneity before weathering and are less affected by weathering in comparison to finer fractions. Therefore, for the particle size analyses, we discarded the coarser fractions, and only particle size distributions in finer fractions are shown in Fig. 8. As that figure readily shows, clay and silt fractions increase from zone I to zone II. Interestingly, Shirasu in zone IIb is poorer in silt and clay fractions than that in zone IIa. This difference could be the effect of segregation of fine fractions from coarser fractions in the formation of clay bands. The clay band from zone IIc is richer in
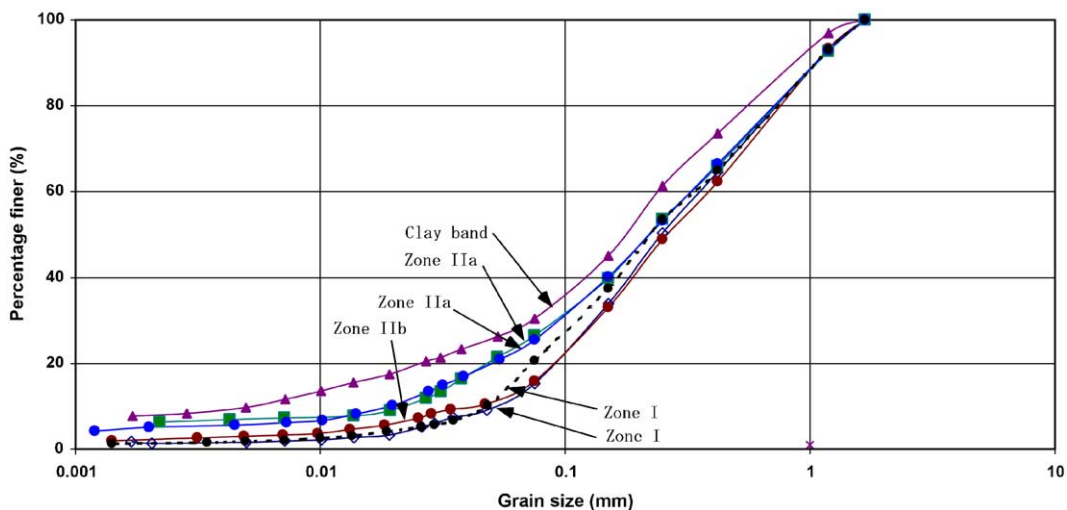
Fig. 8. Particle size distribution.

clay and silt fractions than is Shirasu from the other zones.

3.3. Halloysite and erionite

X-ray analysis was performed for the samples along lines N-3, N-6, T-1, T-2, and T-3. Secondary minerals identified within clay fractions were halloysite and erionite. Halloysite from the study sites changed its basal diffraction peak from 10 Å under the condition of natural moisture content to 7.5 Å when it was dried in room conditions. Fig. 9 shows an example of the change of the 7.5 Å diffraction peaks of halloysite within the clay fraction along a horizontal, ridge-crossing scanning line N-3. It is
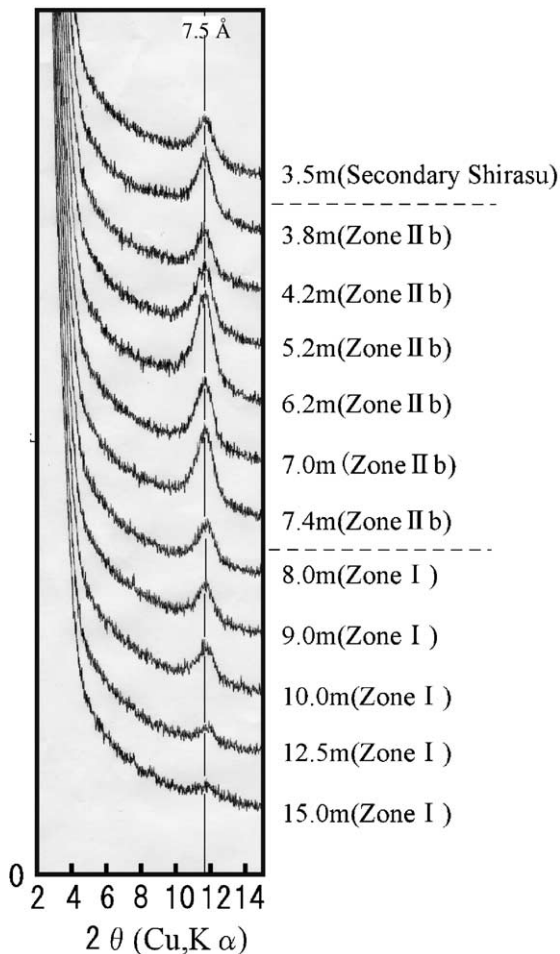
Fig. 9. The change of reflection peaks of halloysite (7.5 Å) along line N-3.

clearly recognized that halloysite is either not contained or poor in the depth of zone I while it is abundant in zone IIb. Halloysite is also abundant in zone IIa but in zone IIc, it is somehow segregated from original grains to form clay bands, so halloysite is abundant in clay bands and is poor outside the clay bands. An increase in the amount of halloysite in the weathering zone of Shirasu was also reported by Kawano and Tomita (1999). Erionite, which is a type of zeolite, was detected within zones IIb and IIc at site T. It is a common alteration mineral of rhyolitic tuff in saline, alkaline lakes, and diagenetic or hydrothermal environments (Hay, 1978), and also has been reported from the weathering zone of Shirasu (Kawano and Tomita, 1999). However, the formative process of erionite is not known as yet.

3.4. Surface textures of glass grains

Surface textures of glass grains are shown in Fig. 10. Glass grains from the weathering zones are rich in dimple-like etch pits with diameters of a few to 5 im, while those from zone I are almost free of these pits. The size and density of these etch pits have never been quantified, but they do not differ much among zones IIa, IIb, and IIc. These dimple-like etch pits are known to be made by the dissolution of glass grains in the laboratory (Yanagisawa et al., 1997) and in the field (Kita et al., 1999; Chigira and Oyama, 1999).

3.5. Matric suction

Matric suction was monitored under a 10-m-high slope inclining 30° at site I. The slope had no trees, and only short grass was grown on it. The slope was underlain by volcanic ash and Shirasu (Fig. 11A). Volcanic ash covered the Shirasu and was thicker in the upper slope. We set tensiometer nests at two points on the slope, points 1 and 2, which were separated by a 5-m interval. First, we drilled a hole with a hand auger to log the geology, then set the porous cups at given depths. At point 1, the top 40-cm interval was occupied by volcanic ash; zone IIb or IIc was found from 40 cm to 1.3 m; IIa was from 1.3 m to 1.7 m; and zone I was deeper than 1.7 m. Because the hand-auger drilling destroyed the soil structure, zones IIb and IIc could not be differentiated. At point 2, the top 1.6 m
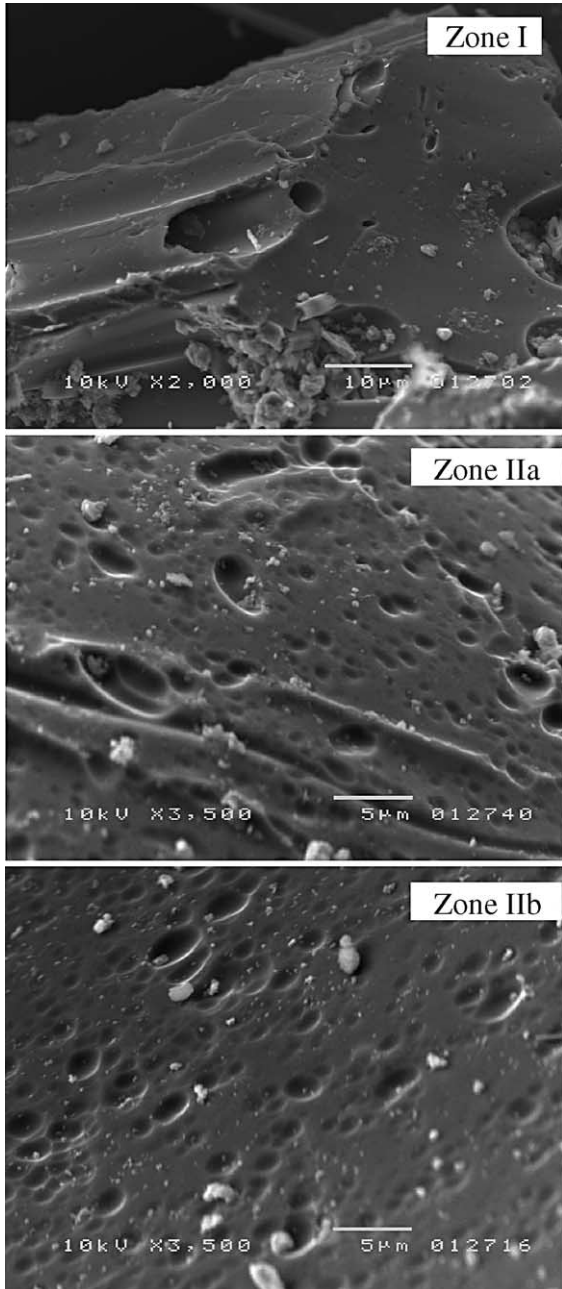
Fig. 10. Surface textures of glass grains observed with scanning electron microscope.

was occupied by volcanic ash, and from 1.6 m to 2.0 m by zone IIb or IIc.

Porous cups were set at depths of 50, 100, 150, and 200 cm at both points, so at point 1, the 50-cm and

100-cm cups were within zone IIb or IIc; the 150-cm cup was within zone IIa; and the 200-cm cup was within zone I. At point 2, the top three cups were within volcanic ash, and only the 200-cm cup was within zone IIb or IIc. The tensiometer tubes were spaced 30 cm from each other.

During the time of monitoring, 23 August to 1 October 2001, we had eight rainfall events, of which the event of 13 and 14 September was monitored successfully to clarify the suction response to rainfall of 170-mm precipitation occurring within 27 h (Fig. 11B). Before this event, the precipitation amounts were 5 mm on 30 August, 51 mm on 2 September, 79.5 mm on 6–7 September, and 37.5 mm on 8 September. After 8 September, there was only 0.5-mm
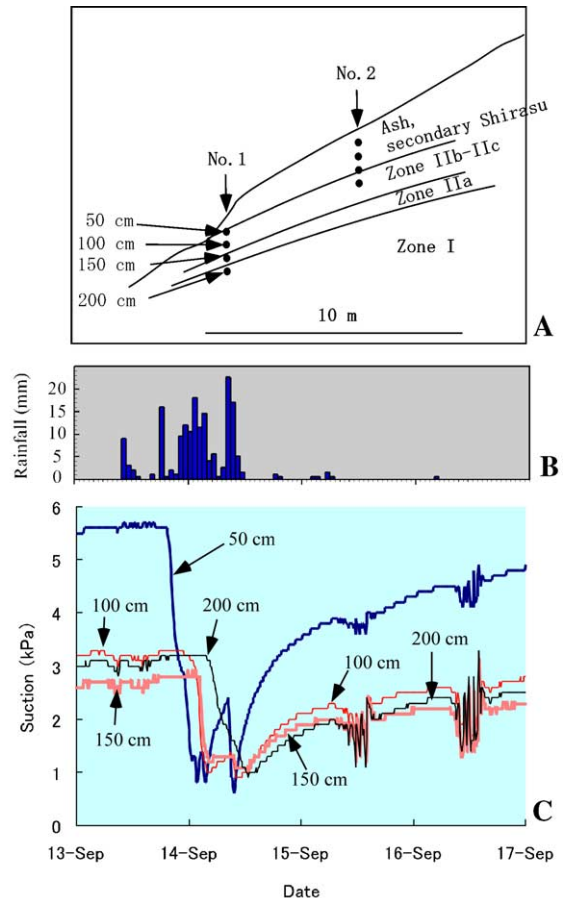
Fig. 11. Geologic cross section of the slope for suction monitoring (A), hourly precipitation (B), and suction change (C) from 13 to 17 September 2001 at point 1.

precipitation before the 13th. The monitoring results at point 1 are shown in Fig. 11C. The tensiometer at the depth of 50 cm responded to the rain first, and then the deeper ones responded successively. In order to clarify the relationship between the weathering profile and the propagation of suction change, matric suctions were plotted versus depth with intervals of 3 or 6 h during the whole event (Fig. 12A) and with 10-min intervals for the time of rapid change, which was from 15 to 27 h from the beginning of rainfall (Fig. 12B). Corresponding precipitation is shown in Fig. 11B. Within the first 15 h of rainfall, suction decreased gradually from 6 kPa to 1 kPa at the depth of 50 cm but remained unchanged (3 kPa) in the deeper parts. Immediately after the suction of 50 cm reached 1 kPa, suctions at the depths of 100 cm and 150 cm almost simultaneously decreased to become 1 kPa at 17 h and 40 min after the beginning of the rain. After this rapid change, suction in the depth of 200 cm

decreased gradually from 3 kPa to 1 kPa within the first 27 h after the beginning of rainfall. This pattern of suction change indicates that there are barriers against water infiltration between the depths of 50 cm and 100 cm and between the depths of 150 cm and 200 cm. The depths of 50 cm and 100 cm are both in zone IIb–c, but the former could be in zone IIc with abundant clay bands, whereas the latter could be in zone IIb with fewer clay bands. An abundance of clay bands thus might be one barrier against water infiltration. Another barrier is between the depths of 150 cm (zone IIa) and 200 cm (zone I). This barrier corresponds to the weathering front, and it will be discussed in the next section. The suction change obtained at point 2 is shown in Fig. 13, which reveals that, first, the 50-cm suction decreased gradually from 9 to 2 kPa, then the 100-cm suction decreased rapidly from 6.5 to 2 kPa, but the 200-cm suction stayed at 3 kPa until 24 h after the rain had begun. The 50-cm
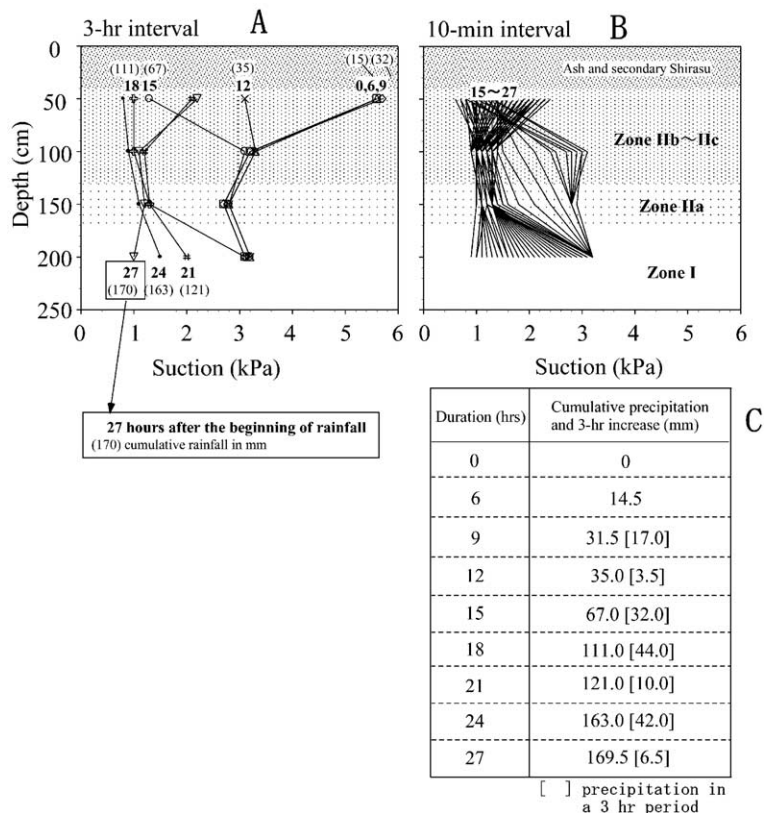
Fig. 12. Suction change at a rainfall event of 170 mm within 27 h from 13 to 17 September 2001. (A) Three- or six-min interval for point 1. (B) Ten-minute interval for point 1. (C) Total precipitation from the beginning of rainfall.
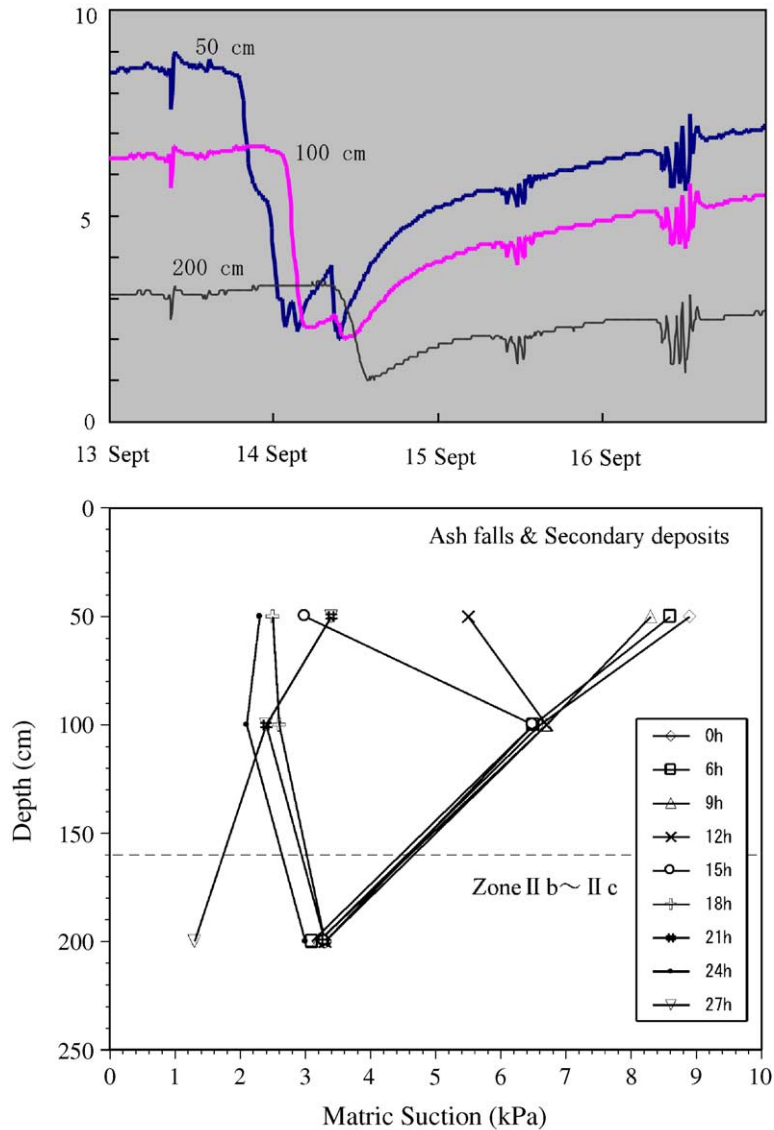
Fig. 13. Suction change observed at point 2.

suction was not measured at this interval because of an accident. The difference in the suction changes between points 1 and 2 is due to the difference in soil structure.

The prohibition of the downward infiltration of water at the weathering front between zones I and IIa may be attributed to the capillary barrier effect provided by the hydrogeological structure made by the weathering. Weathering of Shirasu rearranges and decreases the size of pore spaces as well as grain sizes

by dissolving volcanic glass and forming halloysite, as was discussed in the previous sections. Consequently, a weathering profile has a structure, in which finer grained Shirasu of zone II overlies the coarser grained Shirasu of zone I. When a finer material overlies a coarser material, water does not infiltrate downward through their boundary because of capillary force, which is generally larger for finer material than coarser material (Richards, 1950; Miyazaki, 1988; Ross, 1990). This effect, called the capillary

barrier, has been studied since the 1970s, mainly by theoretical models or by experiments. The present study is the first to monitor a capillary barrier in a natural soil profile.

4. Conceptual model of weathering

The weathering of volcanic glass proceeds mainly by a chemical process, including hydration, dissolution, and clay formation (Petit et al., 1990; Yanagisawa et al., 1997; Kita et al., 1999). Volcanic glass grains are first hydrated and then dissolved (Yanagisawa et al., 1997; Kita et al., 1999). Kita et al. studied the weathering of Aira-Tn ash, which is a regional ash fall ejected contemporaneously with the Ito ignimbrite. They reported that the surface of the volcanic glass grains is dissolved, after which weathering in the field produces dimple-like pits. They also made similar dimple-like pits by dissolving the glass grains with fluoric acid. Such dimple-like pits on acidic volcanic glass grains were also reported from the glass grains contained in the weathering zone of mudstone; they are inferred to be made by dissolution during weathering (Chigira and Oyama, 1999). The dimple-like pits reported by these previous studies have the same morphological features as those described in this paper. That similarity strongly suggests that the pits

were formed when infiltrating water dissolved glass grains. In addition, halloysite concentrating in zones IIa, IIb, and IIc also indicates that it is made by weathering. Halloysite is well known as a weathering product of volcanic materials, such as ash or pumice (Nagasawa, 1979; Chigira, 1982).

Our suction monitoring result provides important information about water infiltration behavior; this information is essential to understand the mechanism of water–rock interaction that makes the weathering profile. Water–rock interaction and water infiltration behavior have been studied from the viewpoint of geochemistry (Lichtner et al., 1996; Lasaga, 1998), but most such studies were based on theoretical study, and almost no studies clarified the relationship between the chemical water–rock interaction and physical water migration behavior on the basis of monitored data in the field. Fig. 14 shows a conceptual model of the infiltration of water into a Shirasu slope. Water within the slope does not infiltrate at a constant rate. Rather, it flows rapidly in some parts and slowly in others, according to the weathering profile. As the suction data showed, water infiltrates through the weathering zone and reaches the weathering front, the bottom of zone II, where its downward infiltration is prohibited by the capillary barrier effect. This barrier increases the contact time between the Shirasu and the water at the weathering
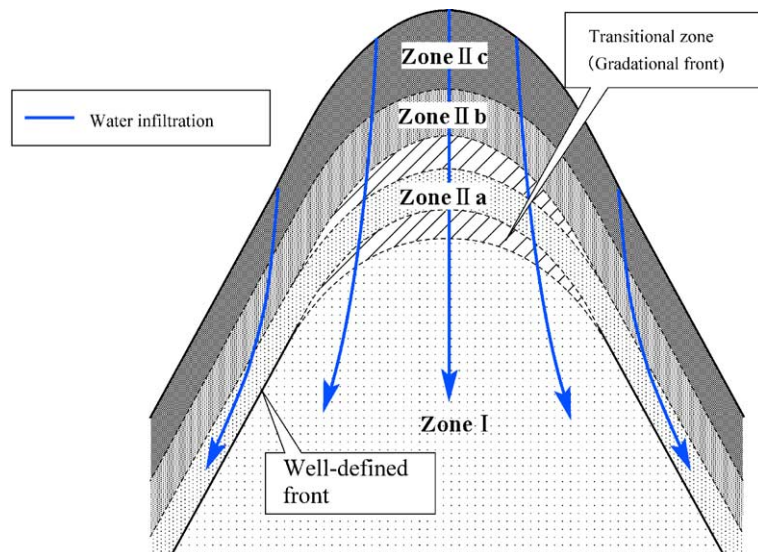
Fig. 14. Conceptual model of water infiltration into Shirasu slope.

front, thus accelerating and concentrating the weathering at the front. If the weathering front is inclined, water does not go down but migrates laterally (Ross, 1990), so the material beneath the weathering front would have less opportunity to come into contact with fresh water. Hence, the weathering front beneath a slope surface is apt to be well defined. On the other hand, the weathering front beneath a ridge top or flat surface has a nearly horizontal weathering front, so water from the ground surface would accumulate on a weathering front because of the capillary barrier, which would be finally breached by the continuous flux of rainwater from the ground surface. The reaction zone is reasonably wider beneath a ridge top than beneath a slope.

At the shallower part of the weathering profile of Shirasu, clay bands are generally abundant. This is typified in zone IIc. The formation of clay bands is attributed to the halloysite formation and to the washout and clogging of clay particles at interstitial pore throats, as described before.

5. The generation and recurrence of landslides

The clay bands and capillary barrier effect discussed above lead to a new concept for the mechanism underlying landslides, as well as for the mechanism of weathering discussed in the previous section. Fig. 15 is a schematic sketch showing the water infiltration behavior and destabilization of a Shirasu slope. Downward infiltration of water is first inhibited by a series of clay bands; some perched water might be made on the clay bands, leading to the weight increase of the weathered zone. After breaching the clay band, water goes down to the weathering front, where it is blocked again, this time by the capillary barrier effect. The increase in weight and the decrease in suction are assumed to be the main causes of landslides, as discussed below.

The conceptual model of water infiltration and landslide occurrence is discussed by examining the stress state at the weathering front. Fig. 16 is a normal stress (σ)–shear stress (τ) graph that shows the stress states at the weathering front parallel to a slope surface while also showing the Mohr–Coulomb failure lines of common fresh Shirasu and weathered Shirasu (Haruyama, 1975). Shirasu and weathered Shirasu described by Haruyama (1975) have soil hardness indices of 26–31 mm and 20–26 mm, respectively, which are in the variation range of Shirasu from zone I and zone II, respectively, at site N of this study. Soil hardness indices from site T are rather lower than these. We presume this is attributable to the extent of consolidation during the time of deposition.
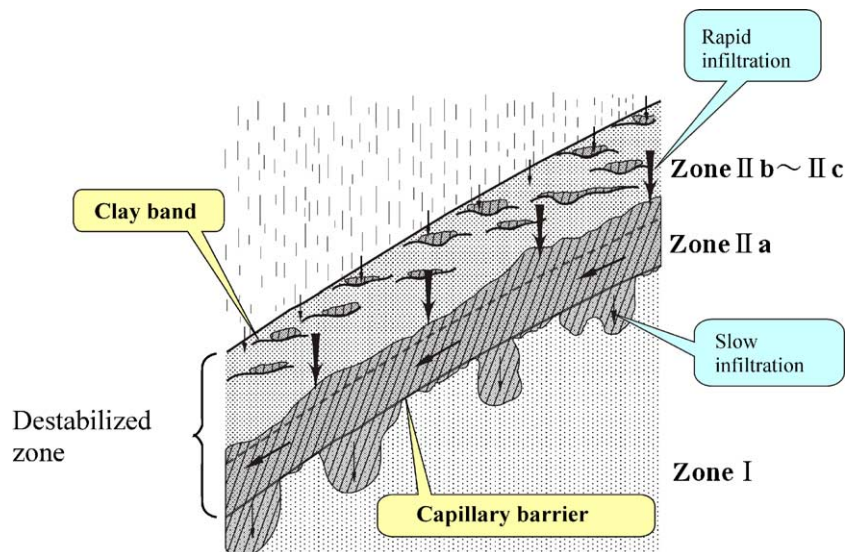
Fig. 15. Schematic sketch of water infiltration and destabilization of a slope.
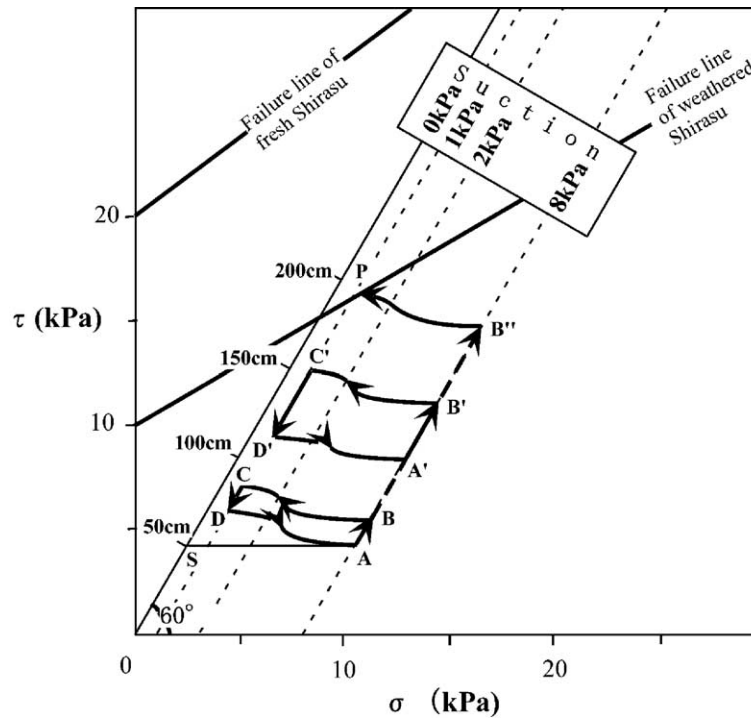
Fig. 16. Sigma–tau graph showing the change of the stress state at the weathering front as weathering proceeds. Mohr–Coulomb fracture lines are shown for the fresh Shirasu and weathered Shirasu.

There are two approaches to dealing with suction in terms of shear strength. Bishop (1960) proposed that suction is added to normal stress in the form,

$$\sigma' = \sigma - u_a + \chi(u_a - u_w),$$

where σ' is effective normal stress, σ is total normal stress, u_a is pore-air pressure, u_w is pore-water pressure, and χ is constant. This is conveniently used, but χ is not easily evaluated, so there is an argument against the use of Bishop's proposal (Toll, 1990). On the other hand, Fredlund and Rahardjo (1993) proposed that the effect of suction on strength is presented as total cohesion c,

$$c = c' + (u_a - u_w)_f \tan \phi^b,$$

in which c is total cohesion, c' is cohesion when suction is zero, u_a is pore-air pressure, u_w is pore-water pressure, $(u_a - u_w)_f$ is suction at the failure, and $\tan \phi^b$ is a parameter to account for the effect of suction. In our study, the effect of suction is incorporated into normal stress, as proposed by

Bishop (1960), because it is convenient to evaluate the stress change and the slope stability on a σ–τ graph with the progress of the weathering and rainfall infiltration.

First assume that the weathering front is at a depth of 0.5 m from a slope surface inclining 60°, and consider the subsequent stress change occurring with the changes in both water content and suction in Shirasu. A 60° inclination is quite common to slopes in the Shirasu area. Weathered Shirasu typically has cohesion up to 10 kPa and an internal friction angle of 30° to 35°, while unweathered Shirasu generally has cohesion up to 20 kPa and an internal friction angle of 38–40° (Haruyama, 1975). Cohesion and the internal friction angle shown in Fig. 16 are 10 kPa and 30° for weathered Shirasu and 20 kPa and 38° for fresh Shirasu. Another parameter used is a dry bulk density of 1 g/cm³. Point S in Fig. 17 indicates the stress on the weathering front under the dry condition without suction. The natural slope, however, has some moisture and hence suction, which is presumed to be 1 to 8–9 kPa from the monitored data at site I. The
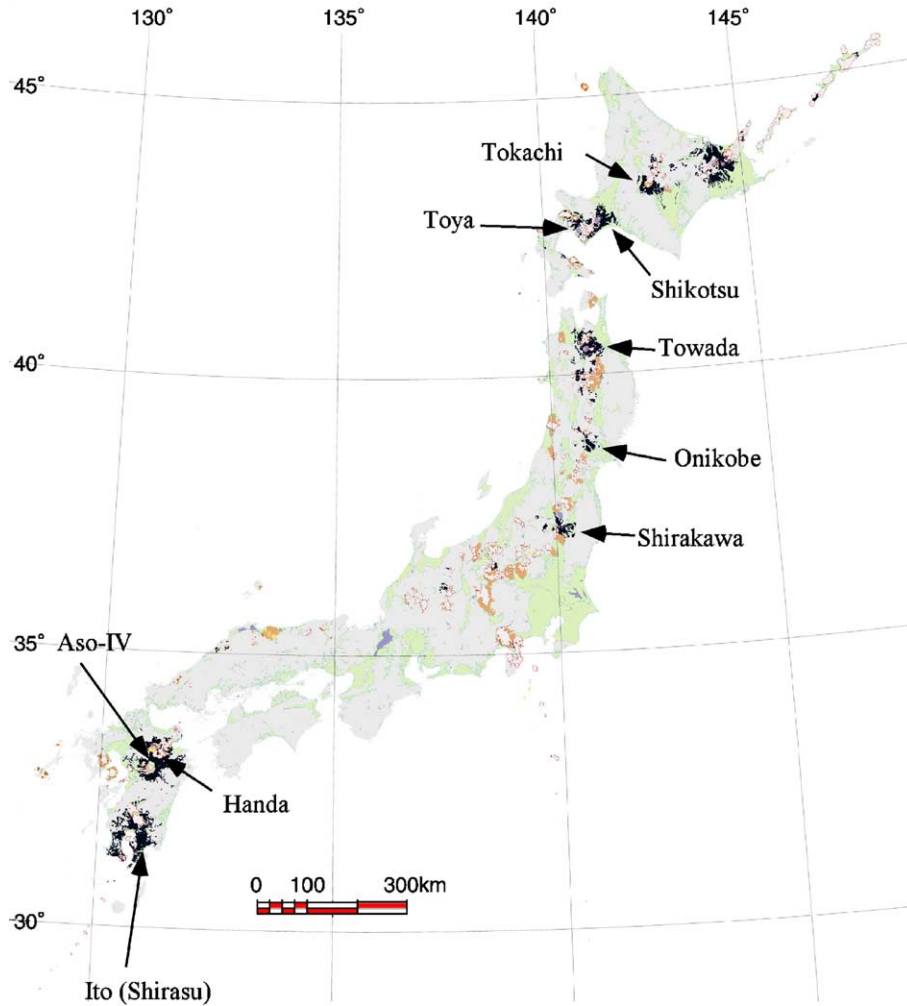
Fig. 17. Distribution of Quaternary ignimbrite in Japan.

stress state with 8 kPa suction is shown by point A. This point would be slightly higher than point S because this Shirasu has some water content. However, since the amount of water is not clear, the presented τ values of S and A are the same. In addition, χ proposed by Bishop (1960) is assumed to be unity for the sake of simplicity. When rainwater comes down from the ground surface, point A moves to B along a line parallel to OS, because the weight of the weathered layer above the weathering front increases. When infiltration water reaches the weathering front, suction at the front starts to decrease. Therefore, the stress state would change from point B to C along a curve. This curve corresponds to the

characteristic curve relating pressure head and moisture content. The two curves are not identical, however, because the weight exerted to the weathering front is the whole weight above the front. Point C is plotted by assuming that the suction after wetting is 1 kPa from the observed data; 1 kPa seems to be the air entry value for Shirasu at the monitored site. After the cessation of rainfall, the weathered layer starts to become drier and lighter, shifting point C to D, from which the suction increases along a curve to get back to point A. The stress path at the weathering front thus forms a hysteresis curve.

As weathering progresses, the weathering front, on which the stress state is discussed, migrates downward

on an order of years, and hence the hysteresis curve of the stress state moves upward on the $\sigma-\tau$ graph, resulting in the increase of the stress level at the weathering front. This means that the stress hysteresis curve at the weathering front becomes closer to the Mohr–Coulomb failure line, as is exemplified in the case of the 100-cm-thick weathering zone in Fig. 16 (points A′, B′, C′, and D′). Stress change by the increase in weight and the decrease in suction during the time of rainfall would finally trigger a landslide. This situation is shown in Fig. 16, where the stress path from point B" hits the Mohr–Coulomb failure line at P at a rainfall event.

6. Implication for other ignimbrite

Shirasu is a typical non-welded ignimbrite, and not a special one, hence the weathering mechanism and the mechanism of landslide generation discussed above can be reasonably applied to other non-welded ignimbrite in humid regions. Our preliminary investigation of weathering profiles of Handa, Shikotsu, and Toya ignimbrite (Fig. 17, (Editorial Board for the Geology of Japanese Island, 1996)) indicated that they are essentially the same as the weathering profile of Shirasu. Handa ignimbrite (32,000 BP) is distributed in northern Kyushu, Japan (Karakida et al., 1992) as well as in Toya (105,000 BP) and Shikotsu (30,000 BP), both in Hokkaido (Kato et al., 1990).

Ignimbrite that has been consolidated by vapor-phase crystallization (Smith and Bailey, 1966; Best and Christiansen, 2001) is not as easily weathered as a non-welded one. It is, however, weathered in humid regions to form a special type of weathering profile that consists of a hydrated zone, an exfoliated zone, and a disintegrated zone from the depth to the ground surface, with each zone having a basal front (Chigira, 2002; Chigira et al., 2002). This type of weathering profile is very different from that of non-welded ignimbrite, described and discussed in this paper. This is because the constituent materials differ between these two types of ignimbrite: vapor-phase-crystallized ignimbrite consists mainly of tridymite and/or cristobalite rather than volcanic glass. A vapor-phase crystallized ignimbrite area in northern Japan (Shirakawa in Fig. 17) was hit by a heavy rainstorm in 1998, leading to numerous landslides. According to

the weathering profile of ignimbrite, the mechanism by which these landslides were generated is assumed to differ from that discussed in this paper. Because of the presence of mechanical discontinuity between the exfoliated zone and the essentially impermeable hydrated zone beneath it, a strongly weathered layer involving the exfoliated and disintegrated zones was probably saturated with water and then slid.

7. Conclusions

The weathering of Shirasu, which is non-welded ignimbrite that erupted 24,500 BP, forms a characteristic weathering profile that consists of three zones from the depth to the ground surface: a softened but not discolored zone (IIa), a softened and discolored zone (IIb), and softened, discolored zones with abundant clay bands. Some zones do not appear at some locations. The softening is caused by the hydration and dissolution of volcanic glass. Clay bands, which are rich in halloysite, develop through the halloysite formation from volcanic glass. The halloysite is transported by water infiltrating through interstitial pores until the halloysite clogs the pore throats.

Suction monitoring across the weathering zone and the fresh zone indicates that downward infiltration of rainwater is first disrupted in the shallower part of a weathering zone by less-permeable clay bands, then again at the weathering front by the capillary barrier effect. This capillary barrier effect explains that weathering proceeds at the front because the contact time between Shirasu and water is assumed to be long at the front. The weathering front is well defined particularly beneath a slope, because water moves along the weathering front laterally when the front is inclined.

The weathering zone of Shirasu thickens in tens of years, and finally slides during rainstorm events. The generation of a landslide would be due to the weight increase and suction decrease in the weathered layer. The increase of the weight is the result of two factors: the abundance of clay bands and the capillary barrier effect. These weight increases and the suction decrease change the stress state at the weathering front to satisfy the Mohr–Coulomb failure criteria.

Acknowledgments

References

Best, M.G., Christiansen, E.H., 2001. Igneous Petrology. Blackwell Science, Massachusetts.

Bishop, A.W., 1960. The principle of effective stress. Publication vol. 32. Norweigan Geotechnical Institute.

Cas, R.A.F., Wright, J.V., 1996. Volcanic Successions, Modern and Ancient. Chapman and Hall, London.

Chigira, M., 1982. Dry debris flow of pyroclastic fall deposits triggered by the 1978 Izu–Oshima–Kinkai earthquake: the "collapsing" landslide at Nanamawari, Mitaka–Iriya, southern Izu Peninsula. Journal of Natural Disaster Science 4, 1–32.

Chigira, M., 1990. A mechanism of chemical weathering of mudstone in a mountainous area. Engineering Geology 29, 119–138.

Chigira, M., 2001. Micro-sheeting of granite and its relationship with landsliding specifically after the heavy rainstorm in June 1999, Hiroshima Prefecture, Japan. Engineering Geology 59, 219–231.

Chigira, M., 2002. Geologic factors contributing to landslide generation in a pyroclastic area: August 1998 Nishigo Village, Japan. Geomorphology 46, 117–128.

Chigira, M., Oyama, T., 1999. Mechanism and effect of chemical weathering of soft sedimentary rocks. Engineering Geology 55, 3–14.

Chigira, M., Sone, K., 1991. Chemical weathering mechanisms and their effects on engineering properties of soft sandstone and conglomerate cemented by zeolite in a mountainous area. Engineering Geology 30, 195–219.

Chigira, M., Nakamoto, M., Nakata, E., 2002. Weathering mechanisms and their effects on the landsliding of ignimbrite subject to vapor-phase crystallization in the Shirakawa pyroclastic flow, northern Japan. Engineering Geology 46, 117–128.

Daily, R.A., Edward, G.G., Sydney Jr., P.C., 1966. Density of rocks. In: Sydney Jr., P.C. (Ed.), Handbook of Physical Constants. The Geological Society of America, New York, pp. 20–26.

Deer, W.A., Howie, R.A., Zussman, J., 1966. An Introduction to the Rock-Forming Minerals. Longman, London.

Editorial Board for the Geology of Japanese Island, 1996. Geology of Japanese island. Maruzen, Tokyo.

Fredlund, D.G., Rahardjo, H., 1993. Soil Mechanics for Unsaturated Soils. John Wiley and Sons, New York.

Geological Society, 1995. Engineering group working party report: the description and classification of weathered rocks for engineering purposes. Quarterly Journal of Engineering Geology 28, 207–242.

Hachinohe, S., Hiraki, N., Suzuki, T., 1999. Rates of weathering and temporal changes in strength of bedrock of marine terraces in Boso Peninsula, Japan. Engineering Geology 55, 29–43.

Haruyama, M., 1975. C and φ—Shirasu-. Tsuchi to Kiso. Japanese Geotechnical Society 23 (7), 67–74 (in Japanese).

Hay, R.L., 1978. Geological occurrence of zeolite. In: Sand, L.B., Mumpton, F.A. (Eds.), Natural Zeolites: Occurrence, Properties, and Use. Pergamon Press, New York.

Karakida, Y., Hayasaka, S., Hase, Y. (Eds.), 1992. Regional Geology of Japan Part 9, KyushuKyoritsu Shuppan, Tokyo (in Japanese).

Kato, M., Katsui, Y., Kitagawa, Y., Matsui, M. (Eds.), 1990. Regional Geology of Japan: Part 1. Hokkaido. Kyoritsu Shuppan, Tokyo (in Japanese).

Kawano, M., Tomita, K., 1999. Formation and evolution of weathering products in rhyolitic pyroclastic flow deposits, southern Kyushu, Japan. Journal of the Geological Society of Japan 105, 699–710 (in Japanese with English abstract).

Kita, S., Yamamoto, H., Furusawa, A., 1999. Weathering of Aira-Tn Ash. Journal of the Geological Society of Japan 105, 410–420 (in Japanese with English abstract).

Lasaga, A.C., 1998. Kinetic theory in the earth sciences. Princeton Univ. Press, Princeton, NJ.

Lichtner, P.C., Steefel, C.I., Oelkers, E.H. (Eds.), 1996. Reactive transport in porous media, Reviews in Mineralogy, vol. 34. Mineralogical Society of America, Washington, DC.

Miyazaki, T., 1988. Water flow in unsaturated soil in layered slopes. Journal of Hydrology 102, 201–214.

Moye, D.G., 1955. Engineering geology for the Snowy Mountain scheme. Journal of the Institution of Engineers, Australia 27, 287–298.

Nagasawa, K., 1979. Weathering of volcanic ash and other pyroclastic materials. In: Sudo, T., Shimoda, S. (Eds.), Clays and Clay Minerals in Japan, Developments in Sedimentology vol. 26, pp. 105–125.

Oyama, T., Chigira, M., 1999. Weathering rate of mudstone and tuff on old unlined tunnel walls. Engineering Geology 55, 15–28.

Petit, J.C., Mea, G.D., Dran, J.C., Magonthier, M.C., Mando, P.A., Paccagella, A., 1990. Hydrated-layer formation during dissolution of complex silicate glasses and mine. Geochimica et Cosmochimica Acta 54, 1941–1955.

Phillips, O.M., 1991. Flow and Reaction in Permeable Rocks. Cambridge Univ. Press, New York.

Richards, L.A., 1950. Laws of soil moisture. Transactions American Geophysical Union 31, 750–756.

Ross, B., 1990. The diversion capacity of capillary barriers. Water Resources Research 26, 2625–2629.

Ruxton, B.P., Berry, L., 1957. Weathering of granite and associated erosional features in Hong Kong. Bulletin of the Geological Society of America 68, 1263–1292.

Shimokawa, E., 1984. Natural recovery process of vegetation on landslide scars and landslide periodicity in forested drainage basins. Proceedings of the Symposium on Effects of Forest Land Use on Erosion and Slope Stability, pp. 99–107.

Shimokawa, E., Jitousono, T., Takano, S., 1989. Periodicity of shallow landslide on Shirasu (Ito pyroclastic flow deposits)

steep slopes and prediction of potential landslide sites. Transactions Japanese Geomorphological Union 10, 267–284 (in Japanese with English abstract).

Smith, R.L., Bailey, R.A., 1966. The Bandelier Tuff, a study of ash-flow eruption cycles from zoned magma chambers. Bulletin of Volcanology 29, 83–104.

Toll, D.G., 1990. A framework for unsaturated soil behavior. Geotechnique 40, 31–44.

Yanagisawa, N., Fujimoto, K.N., Kurata, Y., Sanada, N., 1997. Micro FT-IR study of the hydration-layer during dissolution of silica glass. Geochimica et Cosmochimica Acta 61, 1165–1170.

Yokota, S., Iwamatsu, A., 1999. Weathering distribution in a steep slope of soft pyroclastic rocks as an indicator of slope instability. Engineering Geology 55, 57–68.

Yokota, S., Fukuda, T., Iwamatsu, A., Uda, S., Wada, T., Masaki, H., 1997. Infiltration of rainwater from slopes of pyroclastic flow deposits using automated electrical prospecting. In: Wang, S., Marinos, P. (Eds.), Proc. 30th Int'l. Geol. Congr. Brazil, VSP, Utrecht vol. 23, pp. 489–499.

Yokoyama, S., 1999. Rapid formation of river terraces in non-welded ignimbrite along the Hishida River, Kyusyu, Japan. Geomorphology 30, 291–304.